On the intra annual surface height variations due to climate variations in Arctic- Svalbard ☆

Halfdan Pascal Kierulf[*,a,b], Ward van Pelt[c], Leonid Petrov[d], Michael Dähnn[a], Ann-Silje Kirkvik[a], Ove Christian Dahl Omang[a]

[a] *Geodetic Institute, Norwegian Mapping Authority, Hønefoss, Norway.*
[b] *Department of Geosciences, University of Oslo, Oslo, Norway.*
[c] *Department of Earth Sciences, Uppsala University, Uppsala, Sweden*
[d] *NASA Goddard Space Flight Center, Greenbelt, USA*

Abstract

Geodetic stations at the Svalbard archipelago are exposed for a number of weather and climate affects that influence the station coordinates on different temporal and spatial scales. The geodetic stations can therefore be used for studying these effects. This study focus on annual vertical variations in GPS time series and how well different GPS solutions are able to capture the elastic signal from ice, snow and other Non Tidal Loadings (NTL).

We find that the annual signal in different GPS solutions vary with more than 3 mm. Indicating that we have analysis strategy dependent annual signals in the solutions. This make geophysical interpretation of the GPS results difficult. The analysis strategy dependent signal is removed with a Common Mode (CM) filtering where also the signal from NTL is taken into account. Filtering the time series for CM signal improves the consistency between the solutions (amplitude differences ∼1 mm or lower) and the results

☆Intra annual surface variations in Svalbard.

*Corresponding author

are closer to the estimated elastic signal from NTL.

The annual signal at the two station at central Spitsbergen; Longyearbyen and Svea, agree with the loading prediction from ice and snow below the uncertainty level. At the more western stations, Ny-Ålesund and Hornsund, the annual signal is between 0.5 mm and 1.0 mm larger than the prediction.

We have also tested the effect of removing NTL loading from unfiltered and CM filtered time series and we have tested the effect of replacing the global hydrological loading model with a regional model for ice and snow variations.

Removing the loading signal from the unfiltered time series reduce the daily noise scatter with ∼10%, but the annual signal is around 3 mm also after removing the NTL. I.e. the analysis strategy dependent signal dominate the annual signal.

When we remove the loading signal from the CM filtered time series the annual signal is also reduced. Telling us that CM filtering is necessary to reveal local periodic signal when millimeter precision is required. The amplitude of the annual signal is reduced to ∼2 mm using global NTL models. When we refine the global hydrological model with a regional model for ice and snow variations the amplitude of the annual signal is reduced to ∼1 mm.
Key words: GPS, Climate mass balance, Intra annual surface deformations, Non tidal loading, Svalbard

1. Introduction

The Arctic archipelago Svalbard is exposed to climate change phenomena, the temperature is rising, the permafrost is melting, the sea level is rising and

the glaciers are retreating (**?**). Consequences of climate change, like sea-level rise or increased land-uplift, can be observed by geodetic techniques in an accurate geodetic reference frame. On the other hand, these changes challenge the stability of the geodetic reference frame itself, e.g. will the increased land uplift deform the reference frame over time. Knowledge about the interaction between geophysical processes, crustal deformations and reference frame is mandatory to achieve the GGOS2020 goal of a reference frame with a stability of 0.1 mm/yr (**?**)

The geodetic observatory in Ny-Ålesund is one of the core stations in the global geodetic network. It was established during the 1990s with GPS antennas, VLBI telescope, SCG, absolute gravity points and control networks (**?**).

Due to Svalbard's remote location and challenging environmental conditions Ny-Ålesund was for a long time the only site with permanent GPS antennas on the archipelago. **??** studied the gravity signal in Ny-Ålesund and the interaction between gravity changes and uplift. For almost 20 years it has been evident that the uplift in Ny-Ålesund is not linear, but changes with time (e.g. **??**). **?** showed that the uplift changed from year to year and that these variations are very well explained by the changes in the mass balance at the nearby glaciers. **?** found similar change in the gravity rate as in the uplift. **?** showed that topography of glaciers has a significant effect on the gravity rate. The visco-elastic response on the last ice age (**?**) and the visco-elastic response on the glacier retreat after the LIA (**?**) also contribute to the uplift in Ny-Ålesund. In 2005, the Polish research station in Hornsund installed a new GPS antenna. **?** compared results from the stations in Horn-

sund and Ny-Ålesund and demonstrated that both locations have non-linear uplift. All these papers focus mainly on glacier related phenomena with time span ranging from years to decades or thousands of years.

The most prominent variations in snow cover and glacier mass are the annual cycle with accumulation of snow each winter and melting in the short Arctic summer. The crusts elastic response on this seasonal variations give an annual cycle also in the GPS station coordinates. The crust is also exposed for NTL from ATM, NTO and LWS(**??**). The regional signal from ice and snow is not very well modeled in existing LWS models. The CMB model described in **?** gives the variations in RIS based on meteorological models and observations. This CMB model have high spatial and temporal resolution and can be used for studying the annual variations in the vertical component of GPS station coordinates.

? found differences in the annual signal in GPS time series using different softwares and analysis strategies. We find similar differences in this study. Such differences make geophysical interpretation of the results difficult. It also hamper the effect of removing NTL from GPS time series.

The main questions in this paper are: (1) How well can GPS capture the loading signal from RIS at Svalbard? (2) Will refining the LWS models with RIS model improve the loading predictions? To answer these two questions we have studied GPS time series using different analysis strategies. We have also filter our time series for NTL and CM signal to improve the regional precision.

In Section 2 we describe the different data used in this study. We describe the softwares and analysis strategies for geodetic analysis, the time

series analysis, the CM filtering and the different models used for loading predictions. In Section 3, we compare the geodetic results with the loading signal from RIS, and the loadings from ATM, NTO and LWS. Based on this we discuss possibilities and limitations in our solutions for revealing the annual elastic signal. We also study the effect of including RIS in the hydrological models (Subsection 3.2).

2. Data and data analysis

2.1. CMB models

The load from the Svalbard glacier can be modeled in various ways. Areal photographs, climate modeling, satellite altimetry and satellite gravimetry, glacier stakes...more about the methods... Climate modeling is the only way to model the high spatial and temporal variations in the ice masses that are necessary for the study of the sub annual variations in the uplift, which are the main topic of this paper.

Several CMB models exists, (e.g. **???**). .. more about these models– short description.... **?** have longer time span and includes also the variations in snow cover. We have therefore used this model, to compute the local hydrological signal.

2.2. Elastic loading signal

~~The earth crust response on different loadings as an elastic body. Tidal loadings like ocean tide loadings and ocean pole tide are included in the GPS analysis (see Table 1). Non-tidal loadings from ATM, NTO and LWS are normally not included in geodetic analysis. However, they can significantly~~

~~deform the earth crust (?). There are several web based services that can be used to compensate for the non-tidal loadings e.g. `http://massloading.net/` and `http://loading.u-strasbg.fr/`. We have used the ATM loading (geospift) and NTO loading (mpiom06) and LWS loading (merra2) from the first. We name the sum of the signal from ATM, NTO and LWS (without regional ice and snow) for the AOH loading signal~~

~~The hydrological loadings in Arctic areas are dominated by regional signal from ice and snow. Such loadings are not very well modeled in global models. We have consequently used the ice and snow model from ? described in Section 2.1. Based on this model we have used the ? approach to estimate the elastic uplift from RIS. To avoid including the loading signal from ice and snow on Svalbard twice, the regional hydrological signal from Svalbard is computed separately from the merra2 model and removed from the LWS loading prediction.~~

Mass redistribution results in Earth's crust deformation called mass loading (?). Mass loading are caused by the ocean water mass redistribution due to gravitational tides and pole tide (ocean tidal loading), by variations of the atmospheric mass (atmospheric pressure loading), by variations of the bottom ocean pressure caused by ocean circulation (non-tidal ocean loading), and by variations of land water mass stored in soil, snow, and ice (land water storage loading). Mass loading crustal deformations have a typical magnitude at a centimeter level (see e.g. ??). Corr 1

It was shown by ? that the deformation field can found in a form of expansion of the global field of loading mass into spheri-

cal harmonic transform, and the dimensionless coefficients of the transformation that depend on degree called Love numbers can be found by a solution of a system of differential equations. Therefore, when the global pressure field mass redistribution is known, the elastic deformation can be found by expansion of that field into spherical harmonics, scaling the harmonics by Love numbers and performing an inverse spherical harmonics expansion. Corr 2

We used for our work Love numbers computed using REAR software ? for the Earth reference model STW105 (Kustowski et al., 2007), which is an update of PREM (Dziewonski and Anderson, 1981) model. We used time series of mass loading caused by atmospheric pressure loading using the pressure field from the output of NASA numerical weather model MERRA2, ocean tidal loading using the tidal model FES14b, non-tidal ocean model MPIOM06, and the land-water storage loading using the pressure field the output of MERRA2 model that accounts for soil moisture at the depth 0–2 meter and accumulated snow. All loadings were computed using degree-order 2699 spherical harmonics transform and presented at a global grid $2' \times 2'$ with a time step 3 or 6 hours. Then mass loading at a given stations is found by interpolation. The time series of these loadings for all GNSS and VLBI sites that we used for this study are available at the International Mass Loading Service `http://massloading.net` (?). Corr 3

However, MERRA2 numerical whether model is known not adequately describe accumulation and runoff of water, snow, and

ice at glaciers since it does not consider all complexity of glacial dynamics and its resolution, 16x55 km for Svalbard, is insufficient to catch fine details. Therefore, we used regional model WVP driven by climate. The model output provides the height of the melted water equivalent. It has resolution 1×1 km, time step 7 days and runs since 1990.08.05 through 2018.08.26. We have re-gridded the output of the WVP model to a uniform, regular, latitude-longitude grid with a resolution of $30'' \times 30''$. The model value at a given element of the new grid is

Corr 4

$$M_{ij} = \frac{\sum_{ab} M_{ab} \exp(-r_{ij,ab}/D)}{\sum_{ab} \exp(-r_{ij,ab})},$$

where $r_{ij,ab}$ is the distance between grid points i,j and a,b, and D is the kernel distance set to 1 km.

Corr 5

We have computed mass loading at $30'' \times 30''$ grid from the WVP output, using spherical harmonic expansion degree/order 10799. This unusually high resolution was used to correctly model the signal at stations that are located close to the edge of glaciers.

Corr 6

However, it is not sufficient to replace the land-water storage loading computed on the basis of MERRA model with the mass loading computed on the basis of WVP model. Crustal deformation at a given point is affected not only by mass loading from the surrounding area in the close vicinity, but from the remote area as well. Therefore, in order to account for loading displace-

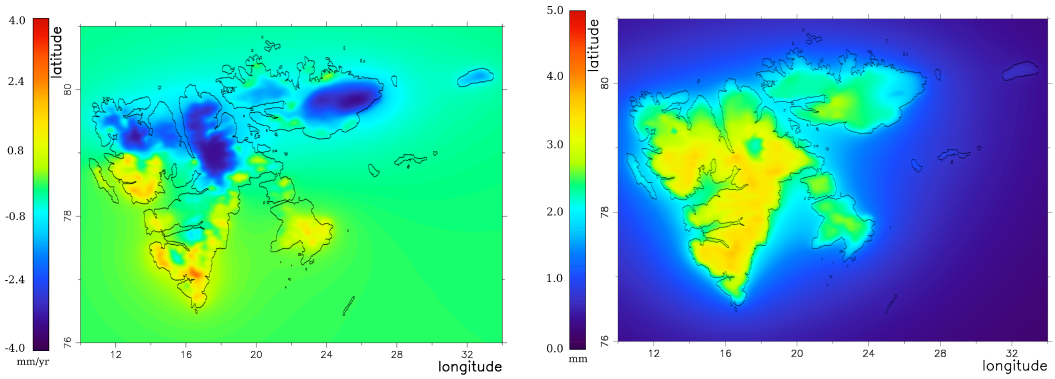

Figure 1: *Left*: Rate of change of the the crustal deformations due land-water mass loading according to WVP model. Important: WVP model does not account for mass loss due to glacier ablation and calving. *Right*: Amplitude of the annual crust deformation due to glacier mass variations according to WVP model.

ment caused by mass redistribution from the area beyond Svalbard archipelago, we computed an additional series of land water storage mass loading using MERRA2 model that was set to zero everywhere, except latitude $76° < \phi < 81°$ and longitude $10° < \lambda < 34°$. That area includes Svalbard archipelago. The total land-water mass-loading displacement is $D_{merra} - D_{merra,svalbrard} + D_{WVP}$. Corr 7

Figure 1 shows the high resolution maps of the rate and the amplitude of annual signal in crustal deformation caused by the accumulated water mass change at Svalbard archipelago according to WVP model. It should be noted that WVP model accounts only for climatic forcing and does not account for glacial ablation and calving. These two signals result in glacial mass removal which causes land uplift. Corr 8

~~The total loading signals (sum of loading from AOH and RIS) for Ny-Ålesund~~

Figure 2: GPS network on Svalbard

~~and Bear Island are included in Table 3. The loadings for all the different loading models are include in the Appendix, Table 6.~~

~~Data from the VLBI- and SCG-instrument in Ny-Ålesund are included in this study (see Section 2.4 and 2.5), as well as models for NTL (See Section 2.2) including a detailed CMB model for ice and snow on Svalbard (see Section 2.1).~~

2.3. GPS data analysis

In this study we uses 30 seconds RINEX data from five permanent GPS stations on Spitsbergen, the main island of Svalbard and one station on Bear Island (BJOS) 240 km south of Spitsbergen (see Figure 2). All these stations are located close to existing settlements with infrastructure like power supply and communication. We have also used data from a station named HAGN located at a nunatak in the middle of the glacier Kongsvegen 30 km southeast of Ny-Ålesund. This station is powered by solar panels and batteries. In the dark season, HAGN only record data for 24 hours once a week to save power until the sun is back. Data from the station is downloaded on a field trip once a year.

Data from the GPS stations at Svalbard are analyzed with the program packages GAMIT/GLOBK (**?**) and GipsyX (**?**). The GipsyX software is using undifferentiated observations and the solution are directly realized in ITRF2014 (**?**) through the JPL orbit and clock products. GAMIT software is using double difference observations. To ensure a good global realization in ITRF2014 of the Gamit solution a global network of approximately 90

global IGS stations were analyzed and combined with the Svalbard stations before transforming to ITRF2014. Daily coordinate time series are extracted from these solutions.

The two stations in Ny-Ålesund belong to the IGS-network and are analyzed by several institutions, e.g. UNR (**?**), JPL (**?**) and SOPAC(**?**). NYAL and NYA1 are also included in the latest ITRF (**?**) solution. Key parameters for the different analysis strategies are included in Table 1.

Table 1: GPS analysis strategies. *The upper three are the strategies used for the processing for this paper, the lower three are the strategies for the external analyses included for comparison.(*) Elevation dependent site by site functions, based on actual observations.*

	GAMIT-NMA	GipsyX-FID	GipsyX-NNR
Orbit and clock product	Estimated	JPL fiducial	JPL-NNR
Elevation angle cutoff	10 degree	7 degree	7 degree
Elevation dependent weighting	$\sigma^2 = a^2 + b^2/sin(E)^2$ (*)	$\sigma^2 = 1/\sqrt{sin(E)}$	$\sigma^2 = 1/\sqrt{sin(E)}$
Troposphere mapping function	VMF1	VMF1	VMF1
2nd order ionosphere model	IONEX from CODE	IONEX from JPL	IONEX from JPL
Ocean loading	FES2004	FES2004	FES2004
Ocean pole tide model	IERS 2010	IERS 2010	IERS 2010
Ambiguity	resolved	resolved	resolved
	GAMIT-SOPAC	GipsyX-UNR	GipsyX-JPL
Orbit and clock product	Estimated	JPL-NNR	JPL-NNR
Elevation angle cutoff	10 degree	7 degree	7 degree
Elevation dependent weighting	$\sigma^2 = a^2 + b^2/sin(E)^2$ (*)	$\sigma^2 = 1/sin(E)$	$\sigma^2 = 1/\sqrt{sin(E)}$
Troposphere mapping function	VMF1	VMF1	GPT2w
2nd order ionosphere model	IONEX from IGS	IONEX from JPL	IONEX from JPL
Ocean loading	FES2004	FES2004	FES2004
Ocean pole tide model	IERS 2010	IERS 2010	not applied
Ambiguity	resolved	resolved	resolved

The time series are analyzed with Hector (**?**) software. We have opt to include trend, annual and semi-annual harmonics in the time series analysis using the model function:

$$h(t) = A + Bt + \sum_{j=1}^{2} C_j cos(j2\pi t - \phi_j), \tag{1}$$

where A is the constant term, B is the rate, C_j is the amplitudes of the

Figure 3: Time series for Svalbard. *The time series are Gamit-NMA NYA1 (upper left) and BJOS (lower left), loading (AOH pluss RIS) in Ny-Ålesund (upper right) and gravity from the SCG in Ny-Ålesund (lower right).*

harmonic constituents, and ϕ_j is the corresponding phases. We have assumed that the temporal correlation in the time series are a combination of white noise and flicker noise. We have used used data from 2010-01-01 until 2018-10-01 in all results and comparisons. This limited time period ensure that we have the same time period for all the stations (except HAGN which was established in 2013), no breaks due to equipment shift in the time series and the time series are overlapping with the CMB model (see Section 2.1).

2.4. VLBI

~~The results for the VLBI antennae in Ny-Ålesund, NYALES20, were obtained using the geodetic analysis software Where~~. The VLBI station NYALES20 participated in ~~approximately 2000 24 hour session from 1994 to the beginning of 2020~~ **2183 twenty four hour observing sessions since 1994.10.04 through 2020.10.19**. ~~These sessions were individually analyzed with the following approach:~~ **We ran several solutions.** Corr 9 Corr 10

Solution s1 was obtained using the geodetic analysis software Where (see ?, for more details). VLBI observing sessions were individually analyzed with the following approach: a priori station coordinates were taken from ITRF2014 including the post-seismic deformation models or VTRF2019d for newer stations. All station positions were estimated with a tight NNR/NNT constraint to the ITRF2014. A priori radio source coordinates were taken from the ICRF3 S/X catalog and corrected for Corr 11 Corr 12

the galactic aberration. The source coordinates were not estimated. A priori earth orientation parameters were taken from the C04 combined EOP series consistent with ITRF2014. The polar motion, polar motion rate, UTC-UT1, LOD and celestial pole offsets were then estimated. In addition, troposphere and clock parameters had to be estimated. The VMF1 model was used for the troposphere, TPXO7.2 model was used for the tidal ocean loading. No model for higher order ionosphere is applied.

Solution s2 was obtained using NASA VLBI analysis software suite pSolve. The data were processed in a global reference frame free solution. Source position, station positions, station velocity, harmonic position variations at annual, semi-annual, diurnal, semi-diurnal frequencies of all the stations, as a global parameters in a single least square solution using all dual-band ionosphere-free combinations of VLBI group delays since 1980.04.12 through 2020.12.07, in total 14.8 million observations. There are 28 stations that have discontinuities due to seismic events or station repair. These discontinuities and associated non-linear motion was modeled with B-spline with multiple knots and the coefficients of the B-splines were treated as global parameters. In addition to global parameters, the Earth orientation parameters, pole coordinates, UT1, their first time derivatives, as well as daily nutation offsets are estimated for each observation session individually. Atmospheric zenith path delay and clock function are modeled with B-spline of the 1st degree with time span 60 and 20 minutes respectively. So-called minimum constraints on station positions and

velocities and source coordinates were imposed to invert the matrix of the incomplete rank. These constraints require that the net translation and rotation station positions and velocities of a subset of stations be the same as in ITRF2000 catalogue and net rotation of the so-called 212 defining sources be the same as in ICRF. It should be noted that s2 solution is independent on the choice of the a priori reference frame, i.e. change in the a priori position does not affect results. Corr 13

The data reduction model included modeling thermal variation of all antennas, oceanic tidal, oceanic non-tidal, atmospheric and land-water mass loading with one exception: $D_{merra} - D_{merra,svalbrard}$ land water storage loading was used for station NYALES20. Corr 14

The VLBI network is small and heterogeneous: different stations participate at different experiment. Therefore, the time series of station position should be treated with a great care: the estimate of the position change of station X affects the position estimate of station Y because of the use of the net translation and net rotation constraints to solve the system of the incomplete rank. An alternative approach to processing time series is estimation of admittance factor. We assume that the time series of the displacement in question d(t) is present in data as $a \cdot d(t)$ where a is the dimensionless parameter called an admittance factor that is assumed constant for the time period of observations. The admittance factor describes which share of the modeled signal is present in observations. Corr 15

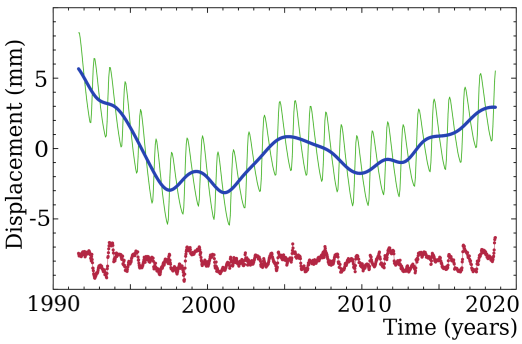

Figure 4: Three constituents of the vertical land water storage mass loading at station NYALES20. The thick blue line shows the interannual variation, the green thin line shows the seasonal component, and red dots in the bottom shows the residual signal. The residual signal is artificially shifted by -8mm. The linear trend is removed and shown.

In solution s3 with did not estimated annual and semi-annual variations of NYALES20 positions, and estimated admittance factors for the up, east, and north components of the $D_{WVP}(t)$ mass loading time series. The results are presented in 2 in column ADM_TOT. Corr 16

We noticed that seasonal crustal deformations of NYALES20 positions are periodic but harmonic. The shape of these variations is stable with time. We decomposed the mass loading signal into four components: periodic seasonal, interannual, linear trend, and residuals. The constituents of this expansion for NYALES20 are shown in Figure 4. Then we estimated the admittance factor for the seasonal and interannual variations separately in s4 solution. We wanted to see with signal is recovered better. Corr 17

2.5. Gravimetry/SCG

Table 2: Admittance factors of NYALES20 displacements caused by the land water storage mass loading. The first row, ADM_TOT shows the admittance factor estimate from s3 solution of the total mass loading signal. Rows ADM_SEA and ADM_IAV shows estimates of the seasonal and interannual constituents of the loading signal from s4 solution respectively.

Factor	Up	East	North
ADM_TOT	1.38 ± 0.04	0.62 ± 0.05	2.05 ± 0.12
ADM_SEA	1.10 ± 0.05	0.47 ± 0.11	6.10 ± 0.49
ADM_IAV	2.90 ± 0.07	2.44 ± 0.11	1.00 ± 0.15

We use gravity measurements from two SCG instruments covering the period 1999 to 2018 to estimate gravity change. Gravity measurements from 1999 to 2013 and 2014 to 2018 are collected with C039 and iGrav012, respectively. The original gravity measurements have a spacing of 1 second. The 1 second gravity measurements have been re-sampled every minute using a symmetric numerical Finite Impulse Response (FIR) zero phase low-pass filter. Data was then cleaned for outliers and earthquakes and corrected for the effect of air pressure. We also estimated and removed the instrumental drift by comparing to absolute gravity measurements. Finally, we re-sampled the data first every 1 hour using a symmetric FIR zero-phase filter and then to daily values using a flat filter.

2.6. Filtering of Common Mode and elastic loading signal

It is well known that stations in a region can have a spatial correlated signal, so called CM signal (**?**) and that removal of the CM signal can reduce

noise in the time series. The CM signal could come from the GPS analysis strategy and from the strategy for reference frame realization. It could come from mismodeled orbit, clocks or EOPs, or unmodeled large scale hydrology or atmospheric effects. To remove such signal CM filtering, EOF or regional reference frame realization, can be used. All these methods presuppose that we have stations exposed for the same undesirable CM signal. In Arctic areas, we have limited access to nearby stations. All stations on Spitsbergen are exposed to similar signals from the glacier, using one or several of these stations for removal of the CM signal will not only remove the CM signal, but also the real elastic signal from snow and ice.

The station BJOS at Bear Island is located 240 km south of Spitsbergen. It is the closest station outside Spitsbergen. Time series of the BJOS station are used to estimated the CM signal. At the Bear Island the measured annual signal is smaller. Bear Island is a small island surrounded by ocean and the local loading signal from ice and snow is approximately 10% of the signal in Ny-Ålesund (see Tabel 6). The AOH loading signal are at the same level as for the other Svalbard stations.

The CM filtering remove the common error signal in the stations as well as real measured signal at BJOS. If the station at Bear Island has an unique loading signal not present in other Svalbard stations, this unique signal will be erroneously subtracted also from the other stations.

To CM filter a time series where the signal from a loading model is removed, the loading signal for the station(s) used in the CM filtering has to be removed as well. In our case, the loading signal was subtracted both for the BJOS time series before computing the CM signal and for the other Sval-

bard time series before the CM filtering. The final Svalbard time series are cleaned for both the regional CM signal over Svalbard and Bear Island and the estimated load signal. The CM filtered time series for station i is then:

$$H^i_{CM}(t) = H^i_{GPS}(t) - H^i_{LOAD}(t) - CM(t), \tag{2}$$

where H^i_{GPS} is the observed time series, H^i_{LOAD} is the estimated loading signal. CM is the common mode signal. As described earlier we use the time series from BJOS to estimate the CM signal, but since we remove the estimated loading signal from the time series, we have to remove the loading signal from BJOS time series before computing the CM signal. We get:

$$H^i_{CM}(t) = H^i_{GPS}(t) - H^i_{LOAD}(t) - (H^{BJOS}_{GPS}(t) - H^{BJOS}_{LOAD}(t)). \tag{3}$$

3. Results and Discussion

The results from the different GPS solutions in Ny-Ålesund as well as the total loading signal from AOH and RIS are included in Table 3. In addition are results from the NYALES20 VLBI antenna and SCG in Ny-Ålesund included and results from Bear Island. Some of the time series are plotted in Figure 3.

As shown in **?** the uplift in Ny-Ålesund varies from year to year, consequently trends from different time periods can not be compared directly. We have opt to use the time interval 2010 until 2018 for all solutions, except the ITRF20014 solution that ended in 2014. The differences in uplift agree below the uncertainty level.

The annual signal in Ny-Ålesund varies between the solutions both in phase and amplitude (Table 3). This indicates that we have analysis strategy dependent periodic variations in the reference frame realization or the

Table 3: Trend and annual signal in Ny-Ålesund and Bear Island. *The parametres are estimated trend and annual signal estimated using Eq. 1). The results are for different GPS solutions, VLBI, SCG and NTL in Ny-Ålesund and Bear Island. In the VLBI time-series a pure white noise model is assumed. The gravity values (∗) are multiplied with the free air gradient* -0.308 $\mu Gal/mm$. *CM is the CM filtered time series described in Section 2.6. NTL is the elastic loading signal from AOH and RIS.*

Stat	strategy	Trend (mm/yr)	Amp. (mm)	Pha. (deg)
NYA1	Gamit-SOPAC	9.61 +/- 0.62	6.28 +/- 0.64	-51.3
	Gamit-NMA	9.62 +/- 0.62	5.80 +/- 0.64	-13.0
	GipsyX-FID	9.49 +/- 0.69	3.05 +/- 0.70	-45.7
	GipsyX-NNR	9.26 +/- 0.67	2.96 +/- 0.69	-27.4
	GipsyX-UNR	9.27 +/- 0.67	2.91 +/- 0.69	-27.6
	GipsyX-JPL	9.59 +/- 0.65	3.36 +/- 0.66	-12.9
	ITRF2014	9.00 +/- 0.95	4.05 +/- 0.75	-36.2
	Gamit-NMA (CM)	9.55 +/- 0.36	4.07 +/- 0.38	-47.5
	GipsyX-FID (CM)	9.80 +/- 0.31	2.84 +/- 0.34	-54.0
	GipsyX-NNR (CM)	9.86 +/- 0.35	2.91 +/- 0.38	-58.2
NYAL	Gamit-SOPAC	9.41 +/- 0.61	6.24 +/- 0.63	-56.6
	Gamit-NMA	9.57 +/- 0.67	5.22 +/- 0.69	-12.9
	GipsyX-FID	9.34 +/- 0.67	3.45 +/- 0.74	-59.4
	GipsyX-NNR	9.14 +/- 0.66	3.19 +/- 0.68	-39.9
	GipsyX-UNR	9.13 +/- 0.65	3.17 +/- 0.66	-39.9
	GipsyX-JPL	9.39 +/- 0.65	3.44 +/- 0.66	-27.7
	ITRF2014	9.34 +/- 0.98	4.37 +/- 0.78	-47.7
	Gamit-NMA (CM)	9.52 +/- 0.35	3.60 +/- 0.37	-52.9
	GipsyX-FID (CM)	9.67 +/- 0.33	3.34 +/- 0.38	-63.9
	GipsyX-NNR (CM)	9.75 +/- 0.34	3.45 +/- 0.36	-68.1
NYALES20	Where	8.87 +/- 0.17	2.62 +/- 0.80	-67.3
NYAL-SCG		*1.96 +/- 0.50	*11.21 +/- 0.52	*-83.8
Ny-Ålesund	NTL	0.92 +/- 0.30	4.00 +/- 0.32	-82.5
BJOS	Gamit-NMA	0.10 +/- 0.54	3.30 +/- 0.55	32.6
	GipsyX-FID	-0.27 +/- 0.62	0.90 +/- 0.47	21.2
	GipsyX-NNR	-0.47 +/- 0.59	1.63 +/- 0.58	46.1
Bear Island	NTL	-0.04 +/- 0.31	1.99 +/- 0.32	-107.7

GPS analysis. Such variations make direct geophysical interpretation of the periodicity in GPS time series difficult.

The measured annual signal are smaller than the estimated NTL signal for the GipsyX solutions and larger than the estimated NTL signal for the Gamit solutions. The phase of the GPS solutions are delayed relative to the

NTL signal with between one and two and a half month in Ny-Ålesund.

The annual signal found with VLBI has smaller amplitude, but the phase is close to the expected from the loading modeling. LP or ASK, are there VLBI analysis strategy issues that can explain the lower amplitude for VLBI, e.g. the antenna deformation model.

The gravity values are converted from μGal to mm using the free air gradient (-0.308 $\mu Gal/mm$). The phase of the gravity signal is close to the phase of the loading models, while the amplitude is much larger. Unlike VLBI and GPS, gravity measurements are independent of a reference frame. The SCG-instrument in Ny-Ålesund gives a combined signal from three glacier related factors. The visco-elastic response from past ice mass changes, the immediate elastic response on the ongoing ice mass changes and the direct gravitational attraction from the ongoing ice mass changes on the glaciers (see **??**). The two latter have a clear influence on the annual signal. In addition, local hydrology can give a significant annual gravity signal. Quantifying the gravity signal from these hydrological factors are demanding and out of the scope of this paper. However, they are all closely related to local weather phenomena like temperature and precipitation and we assume that they are in phase with the elastic uplift signal. The phase of the SCG time series is therefore a reference frame independent measure of the variations in Ny-Ålesund.

Results from the CM-filtered Ny-Ålesund time series are included in Table 3. The CM-filtered solutions are closer to the expected loading signal and we have less differences between the GipsyX and Gamit solutions.

3.1. Geodynamical interpretation

To study how well the time series are able to capture the loading signal from RIS, we have to remove other known loading signals from the time series. To have a more robust time series in this discussion we have averaged the time series, Gamit-NMA, GipsyX-NNR and GipsyX-FID. Readers interested in the results for the individual analysis strategies can find that in the Appendix.

The signal in $H_{CM}(t)$ time series (Eq. 3) includes all vertical motions not accounted in the loading models or CM filtering, e.g. unmodeled loading, GIA, tectonics and noise. Assuming that the GIA and the tectonic component are linear the left hand side can be written $H_{CM}(t) = LIN(t) + \varepsilon(t)$, where LIN is the linear part and ε contains the noise including unmodeled loadings. Splitting the load signal from AOH and RIS ($H_{LOAD} = H_{AOH} + H_{RIS}$), we can rewrite the equation and get:

$$\begin{aligned} LIN^i(t) + H^i_{RIS}(t) + \varepsilon(t) &= H^i_{GPS}(t) - H^i_{AOH}(t) \\ &- (H^{BJOS}_{GPS}(t) - H^{BJOS}_{AOH}(t) - H^{BJOS}_{RIS}(t)), \quad (4) \end{aligned}$$

i.e. we have isolated the linear part and the elastic signal from RIS as a sum of known terms.

The annual periodic signal and the linear rate for the time series in Eq. 4 are included in Table 4 together with the elastic signal from RIS. Detailed results for the individual GPS solutions are included in the Appendix Table 7.

The amplitudes of the estimated loading signal from RIS varies with the amount of surrounding glaciers and land masses. The station HAGN in the middle of the glacier Kongsvegen has the largest estimated annual loading

Figure 5: GPS time series for the vertical component of the permanent stations on Svalbard based on Gamit-NMA. *The time series are filtered with the CM-filtering approach described in the text. The absolute level of the y-axis is arbitrary.*

signal, while the western most stations NYAL/NYA1 and HORN have the smallest. The GPS stations SVES and LYRS are localized in central parts of Svalbard and here the measured annual signal agrees with the estimated loading signal. For the stations closest to the west coast NYAL, NYA1 and HORN the measured amplitude are larger than expected form the variations in RIS (~ 0.7 mm, ~ 1.0 mm and ~ 0.5 mm resp.). This might be due to less precision of the CMB models in the more varying coastal climate. The more coastal glaciers have often more dynamic behavior which might increase the seasonal signal, for instance with increased ice calving in the melting season.

The phase of the loading signal from RIS varies with only a few days over Svalbard and correspond to a maximal uplift in mid-October. The phase of the GPS time series agree with the RIS signal from the CMB models within a few weeks.

3.2. CMB models and time series

In the previous section we examined how the different GPS time series were able to capture elastic loading signal from local ice and snow changes. In this paragraph we will discus the effect of removing the loading signal from the time series both on the unfiltered time series and the CM filtered time series. We will in particular look at the effect of replacing the global hydrological model with a regional CMB model. In the discussion we use the average time series from the GPS solutions; Gamit-NMA, GipsyX-FID and

Table 4: Vertical rate and annual signal for GPS stations at Svalbard. *RIS are the elastic loading signal from ice and snow. GPS-CM is the time series using Eq. 4.*

NYA1	GPS-CM	9.74 +/- 0.27	3.37 +/- 0.29	-56.5
	RIS	0.93 +/- 0.03	2.66 +/- 0.03	-81.8
NYAL	GPS-CM	9.57 +/- 0.27	3.63 +/- 0.29	-67.9
	RIS	0.93 +/- 0.03	2.66 +/- 0.03	-81.8
HAGN	GPS-CM	11.95 +/- 0.56	4.29 +/- 0.65	-50.3
	RIS	1.81 +/- 0.04	3.73 +/- 0.04	-80.1
LYRS	GPS-CM	8.16 +/- 0.42	3.21 +/- 0.45	-80.8
	RIS	0.83 +/- 0.03	3.21 +/- 0.03	-83.2
SVES	GPS-CM	6.21 +/- 0.45	3.37 +/- 0.47	-96.8
	RIS	0.86 +/- 0.04	3.53 +/- 0.04	-81.9
HORN	GPS-CM	9.45 +/- 0.27	3.21 +/- 0.30	-60.1
	RIS	1.93 +/- 0.03	2.69 +/- 0.03	-77.0

GipsyX-NNR. Due to limited observations during winter the HAGN time series are not directly comparable with the other time series and therefore not included in this discussion.

We have tested three models for the loading: (1) no-loading, (2) ATM, NTO and the total LWS signal from merra2 model and (3) AOH and RIS loading (the total loading from ATM, NTO and LWS, but where the regional signal in merra2 is replaced with the RIS signal in the CMB model). We have used the unfiltered time series:

$$H^i_{UN}(t) = H^i_{GPS}(t) - H^i_{LOAD}(t), \tag{5}$$

and time series using the CM filtering from Eq. 3.

The H_{UN} in Eq. 5 and H_{CM} in Eq. 3 contain the remaining unmodeled signal in the time series like linear trend (from e.g. GIA and tectonics) and noise including unmodeled loading signals, $H_{UN/CM}(t) = LIN(t) + \varepsilon(t)$. To examine the quality of the time series using different filtering and loading models we estimate the RMS and periodicity of the noise time series $\varepsilon(t)$. A periodic signal in $\varepsilon(t)$ imply remaining unmodeled periodic signal and the RMS the remaining noise. The results for the averaged time series are included in Table 5. Results for the individual solutions are included in Table 8 in the Appendix.

Table 5: Yearly amplitude and RMS in the time series. *In each column the three parameters are amplitude of yearly signal, RMS of the time series and changes in RMS relative the unfiltered time series. The numbers are in mm. The first column is the unfiltered time series. The second column is after removal of the global loadings models (1). The third is after removal of global loadings, but where the regional HYD model is replaced with the regional RIS model (3). The fourth, fifth and sixth column is similar to the first, second and third, but using CM-filtering (Eq. 3).*

Station	UN-(1)	UN-(2)	UN-(3)	CM-(1)	CM-(2)	CM-(3)
BJOS	1.3 / 4.9(0%)	2.9 / 4.1(-16%)	3.0 / 4.1(-16%)			
NYA1	3.8 / 4.6(0%)	3.7 / 4.0(-13%)	3.7 / 3.9(-16%)	3.4 / 4.7(2%)	2.5 / 4.5(-3%)	1.5 / 4.4(-4%)
NYAL	3.6 / 4.6(0%)	3.1 / 4.1(-12%)	3.0 / 3.9(-15%)	3.4 / 4.7(3%)	2.5 / 4.5(-3%)	1.3 / 4.4(-4%)
LYRS	3.0 / 6.8(0%)	2.4 / 6.3(-8%)	2.9 / 6.2(-10%)	2.9 / 6.7(-1%)	1.7 / 6.6(-3%)	0.6 / 6.6(-4%)
SVES	2.5 / 6.5(0%)	1.7 / 5.8(-9%)	2.8 / 5.7(-11%)	2.9 / 6.3(-2%)	1.5 / 6.1(-5%)	1.1 / 6.0(-7%)
HORN	3.3 / 4.7(0%)	3.3 / 4.1(-14%)	3.4 / 3.8(-20%)	3.0 / 4.7(-0%)	2.4 / 4.5(-5%)	1.0 / 4.3(-9%)

We see that removal of the loading signal reduce the RMS values on average 11%, replacing the regional hydrological signal with a CMB model reduce the RMS with 13%. The improvements for the CM filtered time series are less, 4% and 6%, respectively. The removal of the CM have already removed some of the elastic loading signal and this explain the lower reduction for these series. Both for the unfiltered and the CM filtered time series the RMS

are reduced with 2–3 % when we replace the regional signal in the merra2 with the RIS signal from the CMB model.

The RMSs are very litle affected by the CM filtering (4th vers. 1st column). If the time series used for the CM filtering was uncorrelated with the time series we could except an increase in the RMS with a factor of $\sqrt{2}$ or 41%. Despite the relative long distance and quite different environmental conditions at Bear Island, the residual signal in the BJOS series are correlated with the GPS sites at Spitsbergen.

Removing the loading signal from the observed time series have an effect on the daily noise scatter (RMS), but very little effect on the annual signal. This tells us that removal of the NTL reduce the daily scatter in the GPS time series, but that the periodic signal is not dominated by NTL, but other factors. As we saw in Section 3 this annual signal depends on the analysis strategy. We conclude that we have an analysis strategy dependent effect in the periodic signal.

The amplitude of the time series are reduced after the CM filtering. The amplitude of the annual signal in the CM filtered time series using load models (2) are reduced to 2.1 mm. The largest effects are when we use load model (3) and the CM filtered time series. For this solution the averaged annual loading signal is 1.1 mm, one third of most other combinations of filtering and loading models. The average half annual signal (not included in Table 5) is reduced from 1.0 mm in the unfiltered solution to below 0.5 mm when we combine CM filtering with model (3).

It have a large improving effect on the loading signal replacing the regional hydrological signal in merra2 with the RIS signal. However, this positive

effect is masked by the dominant effect of large scale signal in the GPS solutions.

Note, the climate model used in this study is not able to capture the glacier dynamics like the continuous flow of the ice towards the glacier front or more dramatic phenomena as glacier surging. These dynamic effects give a significant contribution to the total glacier mass balance and therefore the uplift especially for the time scales from years and longer (see e.g. **?**, for some considerations on the effect of different dynamics on the glaciers). The linear elastic uplift signal from the CMB models calculated in this paper is not sufficient to fully describe the elastic uplift from ice and snow changes over longer time scales.

4. Conclusions

In the introduction two questions about GPS results and RIS on Svalbard, were raised: (1) How well can GPS capture the loading signal from RIS at Svalbard? (2) Will refining the LWS models with RIS model improve the loading predictions?

Two answer this questions a network of seven permanent GPS stations were analyzed with different analysis strategies and software. The different time series were studied and compared with loading predictions from ATM, NTO, LWS and RIS.

We found large discrepancies between the different analysis strategies, both in phase and amplitude, while the long term trend was more consistent. I.e. We have large analysis strategy dependent effects in the periodic signal in the GPS time series making geophysical interpretation of the results impossi-

ble. However, by utilizing the nearby station at Bear Island for CM filtering the analysis strategy dependent signal was reduced and the remaining time series agree better.

Before comparing the time-series with the RIS signal the elastic loading from ATM, NTO and LWS were removed. The loadings were removed from the CM signal as well before the CM filtering. The remaining annual signal in the GPS time series agree with the annual signal for the central stations. While the annual signals in the time series for the western most stations are lager than the predictions from the RIS in the CMB model.

We saw a clear reduction in the noise of the time series when refining the LWS loading model with prediction based on RIS. The annual amplitude was reduced from 2.1 mm to 1.1 mm for the CM filtered time series. The positive effect was negligible for the unfiltered time series. I.e. CM filtering is necessary to reveal local periodic signal when millimeter rescission is required.

Acknowledgments

The GPS data from Hornsund (HORN) is provided by the Institute of Geophysics of the Polish Academy of Sciences (IG PAS). Time series from SOPAC, JPL and UNR were used in the study. Thanks to Zuheir Altamimi for providing the ITRF2014 time series for the Ny-Ålesund stations.

REFERENCES

A. Tables

Table 6: NTL vertical variations at GPS stations at Svalbard. *AOH is the sum of the loadings ATM, NTO and HYD. Total load is the sum of AOH and RIS.*

NYA1	ATM	0.14 +/- 0.14	1.02 +/- 0.14	-4.1
	NTO	-0.06 +/- 0.23	0.44 +/- 0.20	167.2
	HYD	-0.11 +/- 0.01	1.40 +/- 0.01	-111.8
	AOH	-0.02 +/- 0.30	1.38 +/- 0.31	-84.7
	Snow	-0.16 +/- 0.01	0.83 +/- 0.01	-89.8
	Ice	1.09 +/- 0.02	1.84 +/- 0.02	-78.3
	RIS	0.93 +/- 0.03	2.66 +/- 0.03	-81.8
	Total loads	0.92 +/- 0.30	4.00 +/- 0.32	-82.5
HAGN	ATM	0.15 +/- 0.16	1.12 +/- 0.17	-3.0
	NTO	-0.07 +/- 0.22	0.44 +/- 0.20	167.7
	HYD	-0.10 +/- 0.01	1.41 +/- 0.01	-111.8
	AOH	-0.01 +/- 0.32	1.39 +/- 0.32	-81.2
	Snow	-0.24 +/- 0.01	0.81 +/- 0.01	-88.3
	Ice	2.05 +/- 0.04	2.92 +/- 0.04	-77.7
	RIS	1.81 +/- 0.04	3.73 +/- 0.04	-80.1
	Total loads	1.80 +/- 0.32	5.06 +/- 0.33	-80.1
LYRS	ATM	0.15 +/- 0.15	1.02 +/- 0.16	-3.9
	NTO	-0.09 +/- 0.22	0.46 +/- 0.20	169.1
	HYD	-0.10 +/- 0.01	1.45 +/- 0.01	-111.9
	AOH	-0.04 +/- 0.31	1.41 +/- 0.32	-88.1
	Snow	-0.06 +/- 0.01	1.35 +/- 0.01	-89.7
	Ice	0.89 +/- 0.02	1.87 +/- 0.02	-78.5
	RIS	0.83 +/- 0.03	3.21 +/- 0.03	-83.2
	Total loads	0.80 +/- 0.31	4.57 +/- 0.33	-84.4
SVES	ATM	0.15 +/- 0.17	1.04 +/- 0.17	-3.5
	NTO	-0.10 +/- 0.22	0.47 +/- 0.20	169.3
	HYD	-0.10 +/- 0.01	1.48 +/- 0.01	-112.0
	AOH	-0.05 +/- 0.32	1.43 +/- 0.33	-88.5
	Snow	-0.10 +/- 0.01	1.13 +/- 0.01	-89.2
	Ice	0.95 +/- 0.03	2.41 +/- 0.03	-78.5
	RIS	0.86 +/- 0.04	3.53 +/- 0.04	-81.9
	Total loads	0.81 +/- 0.33	4.92 +/- 0.34	-83.3
HORN	ATM	0.13 +/- 0.13	0.86 +/- 0.13	-3.5
	NTO	-0.10 +/- 0.23	0.48 +/- 0.21	168.9
	HYD	-0.10 +/- 0.01	1.50 +/- 0.01	-112.0
	AOH	-0.07 +/- 0.30	1.44 +/- 0.31	-95.0
	Snow	-0.02 +/- 0.01	0.50 +/- 0.01	-89.6
	Ice	1.95 +/- 0.03	2.20 +/- 0.03	-74.1
	RIS	1.93 +/- 0.03	2.69 +/- 0.03	-77.0
	Total loads	1.87 +/- 0.31	4.05 +/- 0.32	-82.8
BJOS	ATM	0.10 +/- 0.10	0.54 +/- 0.11	-3.4
	NTO	-0.13 +/- 0.26	0.57 +/- 0.24	175.2
	HYD	-0.11 +/- 0.01	1.74 +/- 0.01	-112.4
	AOH	-0.14 +/- 0.31	1.76 +/- 0.32	-111.7
	Snow	-0.01 +/- 0.00	0.07 +/- 0.00	-84.3
	Ice	0.11 +/- 0.00	0.20 +/- 0.00	-77.0
	RIS	0.10 +/- 0.00	0.27 +/- 0.00	-80.8
	Total loads	-0.04 +/- 0.31	1.99 +/- 0.32	-107.7

Table 7: Vertical rate and annual signal for GPS stations at Svalbard. *RIS are the elastic loading signal from ice and snow. GPS-CM is the time series the using Eq. 4.*

NYA1	Gamit-NMA-CM	9.51 +/- 0.37	4.14 +/- 0.39	-59.6
	GipsyX-NNR-CM	9.82 +/- 0.28	3.20 +/- 0.30	-72.8
	GipsyX-FID-CM	9.75 +/- 0.25	3.03 +/- 0.28	-71.2
	GPS-CM	9.74 +/- 0.27	3.37 +/- 0.29	-56.5
	RIS	0.93 +/- 0.03	2.66 +/- 0.03	-81.8
NYAL	Gamit-NMA-CM	9.46 +/- 0.32	3.74 +/- 0.34	-65.5
	GipsyX-NNR-CM	9.69 +/- 0.27	3.80 +/- 0.29	-78.6
	GipsyX-FID-CM	9.62 +/- 0.24	3.60 +/- 0.29	-77.4
	GPS-CM	9.57 +/- 0.27	3.63 +/- 0.29	-67.9
	RIS	0.93 +/- 0.03	2.66 +/- 0.03	-81.8
HAGN	Gamit-NMA-CM	12.49 +/- 0.63	4.38 +/- 0.68	-78.6
	GipsyX-NNR-CM	12.08 +/- 0.54	4.42 +/- 0.70	-61.6
	GipsyX-FID-CM	12.39 +/- 0.50	4.34 +/- 0.67	-61.6
	GPS-CM	11.95 +/- 0.56	4.29 +/- 0.65	-50.3
	RIS	1.81 +/- 0.04	3.73 +/- 0.04	-80.1
LYRS	Gamit-NMA-CM	7.80 +/- 0.35	3.09 +/- 0.37	-53.4
	GipsyX-NNR-CM	8.20 +/- 0.57	3.87 +/- 0.60	-99.3
	GipsyX-FID-CM	8.26 +/- 0.37	3.00 +/- 0.41	-67.1
	GPS-CM	8.16 +/- 0.42	3.21 +/- 0.45	-80.8
	RIS	0.83 +/- 0.03	3.21 +/- 0.03	-83.2
SVES	Gamit-NMA-CM	6.49 +/- 0.43	3.95 +/- 0.45	-80.6
	GipsyX-NNR-CM	6.27 +/- 0.46	3.59 +/- 0.48	-102.4
	GipsyX-FID-CM	6.21 +/- 0.45	3.46 +/- 0.47	-103.5
	GPS-CM	6.21 +/- 0.45	3.37 +/- 0.47	-96.8
	RIS	0.86 +/- 0.04	3.53 +/- 0.04	-81.9
HORN	Gamit-NMA-CM	9.46 +/- 0.27	3.40 +/- 0.30	-55.3
	GipsyX-NNR-CM	9.59 +/- 0.26	3.66 +/- 0.29	-63.8
	GipsyX-FID-CM	9.52 +/- 0.25	3.58 +/- 0.28	-62.6
	GPS-CM	9.45 +/- 0.27	3.21 +/- 0.30	-60.1
	RIS	1.93 +/- 0.03	2.69 +/- 0.03	-77.0

Table 8: Yearly amplitude and RMS in the time series. *In each column the three parameters are amplitude of yearly signal, RMS of the time series and changes in RMS relative the unfiltered time series. The numbers are in mm. The first column is the unfiltered time series. The second column is after removal of the global loadings models (1). The third is after removal of global loadings, but where the regional HYD model is replaced with the regional RIS model (3). The fourth, fifth and sixth column is similar to the first, second and third, but using CM-filtering (Eq. 3).*

Station	UN-(1)	UN-(2)	UN-(3)	CM-(1)	CM-(2)	CM-(3)
BJOS						
Gamit_NMA	3.3 / 4.3(0%)	4.9 / 4.3(-0%)	5.0 / 4.3(-1%)			
GipsyX_NNR	1.6 / 5.0(0%)	3.3 / 4.2(-15%)	3.4 / 4.2(-15%)			
GipsyX_FID	0.9 / 5.2(0%)	2.2 / 4.3(-17%)	2.3 / 4.3(-17%)			
GPS	1.3 / 4.9(0%)	2.9 / 4.1(-16%)	3.0 / 4.1(-16%)			
NYA1						
Gamit_NMA	5.8 / 4.5(0%)	6.0 / 4.6(3%)	5.8 / 4.5(0%)	4.1 / 4.3(-5%)	3.1 / 4.3(-4%)	2.0 / 4.2(-6%)
GipsyX_NNR	3.0 / 5.1(0%)	3.0 / 4.4(-14%)	3.3 / 4.2(-16%)	2.9 / 5.0(-2%)	2.0 / 4.6(-8%)	0.8 / 4.6(-10%)
GipsyX_FID	3.0 / 5.0(0%)	2.3 / 4.2(-16%)	2.4 / 4.1(-18%)	2.8 / 5.0(0%)	1.9 / 4.8(-5%)	0.7 / 4.7(-6%)
GPS	3.8 / 4.6(0%)	3.7 / 4.0(-13%)	3.7 / 3.9(-16%)	3.4 / 4.7(2%)	2.5 / 4.5(-3%)	1.5 / 4.4(-4%)
NYAL						
Gamit_NMA	5.2 / 4.7(0%)	5.5 / 4.8(1%)	5.3 / 4.7(-1%)	3.6 / 4.2(-11%)	2.7 / 4.1(-13%)	1.4 / 4.1(-14%)
GipsyX_NNR	3.2 / 5.1(0%)	2.7 / 4.4(-13%)	2.7 / 4.3(-16%)	3.5 / 5.1(0%)	2.5 / 4.7(-7%)	1.2 / 4.6(-9%)
GipsyX_FID	3.4 / 4.9(0%)	2.0 / 4.2(-15%)	1.7 / 4.0(-17%)	3.3 / 5.0(3%)	2.3 / 4.7(-4%)	1.1 / 4.6(-6%)
GPS	3.6 / 4.6(0%)	3.1 / 4.1(-12%)	3.0 / 3.9(-15%)	3.4 / 4.7(3%)	2.5 / 4.5(-3%)	1.3 / 4.4(-4%)
LYRS						
Gamit_NMA	5.3 / 4.8(0%)	6.2 / 4.9(3%)	6.4 / 4.9(1%)	3.1 / 4.4(-8%)	2.3 / 4.3(-11%)	1.6 / 4.2(-12%)
GipsyX_NNR	2.5 / 7.8(0%)	1.6 / 7.3(-7%)	2.4 / 7.2(-8%)	3.4 / 7.8(0%)	2.2 / 7.6(-4%)	1.4 / 7.5(-4%)
GipsyX_FID	3.1 / 7.0(0%)	2.6 / 6.5(-7%)	2.9 / 6.4(-8%)	2.9 / 7.0(0%)	1.8 / 6.9(-2%)	0.9 / 6.8(-3%)
GPS	3.0 / 6.8(0%)	2.4 / 6.3(-8%)	2.9 / 6.2(-10%)	2.9 / 6.7(-1%)	1.7 / 6.6(-3%)	0.6 / 6.6(-4%)
SVES						
Gamit_NMA	4.6 / 5.7(0%)	4.8 / 5.7(1%)	4.9 / 5.6(-1%)	3.6 / 5.2(-7%)	2.3 / 5.1(-10%)	0.7 / 4.9(-12%)
GipsyX_NNR	2.2 / 6.9(0%)	1.8 / 6.3(-9%)	3.0 / 6.2(-11%)	3.0 / 6.8(-2%)	1.8 / 6.5(-7%)	1.3 / 6.4(-8%)
GipsyX_FID	2.7 / 6.9(0%)	0.9 / 6.2(-11%)	2.2 / 6.1(-12%)	2.9 / 6.8(-2%)	1.7 / 6.5(-7%)	1.4 / 6.4(-8%)
GPS	2.5 / 6.5(0%)	1.7 / 5.8(-9%)	2.8 / 5.7(-11%)	2.9 / 6.3(-2%)	1.5 / 6.1(-5%)	1.1 / 6.0(-7%)
HORN						
Gamit_NMA	5.6 / 4.9(0%)	6.0 / 5.1(3%)	5.9 / 4.9(-0%)	3.3 / 4.5(-8%)	2.7 / 4.4(-10%)	1.4 / 4.3(-14%)
GipsyX_NNR	3.4 / 4.8(0%)	3.4 / 4.1(-14%)	3.4 / 3.9(-19%)	3.3 / 4.8(1%)	2.9 / 4.5(-5%)	1.2 / 4.3(-10%)
GipsyX_FID	3.5 / 4.8(0%)	2.9 / 4.0(-17%)	2.5 / 3.8(-21%)	3.3 / 4.9(1%)	2.8 / 4.7(-3%)	1.2 / 4.4(-8%)
GPS	3.3 / 4.7(0%)	3.3 / 4.1(-14%)	3.4 / 3.8(-20%)	3.0 / 4.7(-0%)	2.4 / 4.5(-5%)	1.0 / 4.3(-9%)